Artificial intelligence framework to predict wall stress in abdominal aortic aneurysm

Timothy K. Chung[a], **Nathan L. Liang**[d,e], **David A. Vorp**[a,b,c,d,f,g,h,*]

[a]Department of Bioengineering, University of Pittsburgh, Pittsburgh, PA, United States

[b]Department of Mechanical Engineering and Materials Science, University of Pittsburgh, Pittsburgh, PA

[c]McGowan Institute for Regenerative Medicine, University of Pittsburgh, Pittsburgh, PA, United States

[d]Department of Surgery, University of Pittsburgh, Pittsburgh, PA, United States

[e]Division of Vascular Surgery, University of Pittsburgh Medical Center, Pittsburgh, PA, United States

[f]Department of Chemical and Petroleum Engineering, University of Pittsburgh, PA, United States

[g]Department of Cardiothoracic Surgery, University of Pittsburgh, Pittsburgh, PA, United States

[h]Clinical & Translational Sciences Institute, University of Pittsburgh, Pittsburgh, PA, United States

Abstract

Abdominal aortic aneurysms (AAA) have been rigorously investigated to understand when their risk of rupture - which is the 13th leading cause of death in the US – exceeds the risks associated with repair. Clinical intervention occurs when an aneurysm diameter exceeds 5.5 cm, but this "one-size fits all" criterion is insufficient, as it has been reported thatup to a quarter of AAA smaller than 5.5 cm do rupture. Therefore, there is a need for a more reliable, patient-specific, clinical tool to aide in the management of AAA. Biomechanical assessment of AAA is thought to provide critical physical insights to rupture risk, but clinical translataion of biomechanics-based tools has been limited due to the expertise, time, and computational requirements. It was estimated that through 2015, only 348 individual AAA cases have had biomechanical stress analysis performed, suggesting a deficient sample size to make such analysis relevant in the clinic. Artificial intelligence (AI) algorithms offer the potential to increase the throughput of AAA biomechanical analyses by reducing the overall time required to assess the wall stresses in these complex structures using traditional methods. This can be achieved by automatically segmenting regions of interest from medical images and using machine learning models to predict wall stresses of AAA. In this study, we present an automated AI-based methodology to predict the biomechanical wall stresses for individual AAA. The predictions using this approach were

*Correspondence author. vorp@pitt.edu (D.A. Vorp).

completed in a significantly less amount of time compared to a more traditional approach (~4 hours vs 20 seconds).

Keywords

Abdominal aortic aneurysm; Artificial intelligence; Machine learning; Stress analysis; Finite element analysis; Automation

1. Introduction

Abdominal aortic aneurysm (AAA) is a localized dilatation of the aorta that if left untreated may rupture, an often-fatal cardiovascular event associated with a 90% mortality rate (Vorp, 2009). Currently, clinicians will intervene when a patient's aneurysm exceeds a maximum diameter of 5.5 cm for men and 5.0 cm for women. However, it has been reported that aneurysms that are smaller than this cut-off still rupture at significant rates from 13 to 23.4% (Kontopodis et al., 2016; Vorp, 2009). To better assess rupture risk, there has been considerable research efforts in the field of biomechanics with the aim of replacing this 50-year-old maximum diameter criterion. These studies have included experimentally measuring the biomechanical behavior of the AAA wall to develop material models (Raghavan and Vorp, 2000, Vande Geest et al., 2006, Martino, S., and Vorp, 2003, Holzapfel, 2006, Sacks and Sun, 2003, Tierney, Callanan, and McGloughlin, 2012) and performing computational finite element analysis (FEA) simulations of 3D reconstructed AAA geometries to assess transmural wall stresses (Vande Geest et al., 2006, Raghavan et al., 2000, Vorp, 2007, Truijers et al., 2007, Fillinger et al., 2002, Chung et al., 2017).

The traditional workflow for FEA wall stress analysis of a patient-specific AAA includes acquiring a computed tomography (CT) angiogram image stack, performing tedious image segmentation and 3D reconstruction of the aneurysm wall and lumen, appropriately meshing the reconstructed aneurysm geometry, assigning material properties from experimentally measured material models, and applying boundary conditions including pressure loads on the surface of the lumen (Fig. 1A) (Vande Geest et al., 2006, Raghavan et al., 2000, Fillinger et al., 2002, Raghavan et al., 2005, Fillinger et al., 2003, Vande Geest, 2005). Clinical adoption of biomechanical assessments of AAA has been slow, due in part to the tediousness of this workflow, which often requires a trained biomechanics expert, and the need for expensive FEA software. This is evident in a 2015 survey performed by Khosla et al., where it was reported that there has been a total of only 348 patient-specific AAA models reported in the literature spanning 20 years, with most of them already clinically sized (> 5.0 cm) (Khosla, Morris, and Moxon, 2015).

There have been reports examining correlations of key quantifiable AAA morphological features with wall stresses to better understand their interplay. Morphological indices studied have included localized principal curvatures (Sacks et al., 1999, Martufi et al., 2009) and mean curvatures (Sacks et al., 1999) of the AAA wall surface, asymmetry (Doyle et al., 2009), aneurysm centerline tortuosity (Sacks et al., 1999, Georgakarakos et al., 2010), and AAA maximum diameter (Raghavan et al., 2000, Shum et al., 2011, Vorp, Raghavan, and Webster, 1998) that are measured objectively through algorithms. However, there is

significant variability when reporting biomechanical wall stresses (peak and mean) of AAA based on how the finite element model was defined and constructed. Differences in aneurysm models include variations of the material model used for the aneurysm wall (e.g., isotropic; Raghavan and Vorp, 2000, Vande Geest, 2005, Raghavan, Webster, and Vorp, 1996) or anisotropic (Vande Geest, 2005, Vande Geest et al., 2008)), the presence or absence of the intraluminal thrombus (ILT (Wang et al., 2002)), the use of ideal systolic blood pressure (120 mmHg) or patient-specific blood pressure (Vande Geest et al., 2006, Truijers et al., 2007, Fillinger et al., 2003, Maier et al., 2010), and the presence of thrombus (ILT). Some studies do not consider the ILT (Truijers et al., 2007, Fillinger et al., 2002), raising the possibility that the calculated wall stress magnitudes and distributions are inaccurate (Martino, S., and Vorp, 2003, Vande Geest et al., 2008, Reeps et al., 2013).

Continual advancements in artificial intelligence (AI) algorithms and software tools have provided methods to perform automated image segmentation using U-NETs, a type of convolutional neural network (CNN) optimized for biomedical image sets (Martufi et al., 2009, Zhang, Kheyfets, and Finol, 2013, López-Linares et al., 2019, Wang et al., 2018) and for improved machine learning (ML) based regression models for accurate prediction (Chen, 2016, Olson and Moore, 2019). A few groups have demonstrated that CNN can be used for reliable segmentation of AAA image sets to provide volume reconstructions on axial CT image stacks for the extraction of ILT, the aneurysm wall and the lumen (López-Linares et al., 2019, Wang et al., 2018, Ronneberger, Fischer, and Brox, 2015). Using a U-NET can alleviate the need for tedious manual segmentation, which can facilitate automation of biomechanical stress analyses, and potentially lead to higher throughput analyses of larger clinical imaging datasets.

In this paper, we present for the first time an AI framework to predict the biomechanical wall stresses of AAA resulting in decreased processing time and increased throughput. The AI framework allows us to perform automatic CT image segmentation, 3D geometric reconstruction and prediction of biomechanical wall stresses (Fig. 1B) based on localized morphological indices and compare the results with those obtained via traditional FEA. The proposed AI framework would allow for high-throughput studies of AAA medical images, reduce the overall energy consumption required to perform stress analysis, and minimize the expertise required to perform computational analyses.

2. Methods

2.1. Biomechanical analysis overview

A total of ten computed tomography angiogram (CT) image set files in Digital Imaging and Communication (DICOM) format were used for this study and were anonymized using an honest broker following an approved IRB protocol at the University of Pittsburgh (protocol #PRO13080334). Our previously described methods (Martino, S., and Vorp, 2003, Raghavan et al., 2000, Vorp, 2007) (Fig. 1A) were used to manually segment regions of interest (ROI) from the CT image sets, reconstruct the lumen and wall geometries from point clouds, perform 2D and 3D meshing in ANSYS ICEM (Ansys Inc., Canonsburg, PA), prepare an Abaqus input file using an in-house MATLAB (Mathworks Inc., Natick, MA.) script, and perform simulations in Abaqus Standard (Dassault Systemés, Providence, RI).

Post-processing was performed for each aneurysm to extract the von Mises wall stresses (N/cm^2) for each wall node and a heat map was generated to be visualized in Paraview (Kitware Inc., Clifton Park, NY). Wall stresses calculated using Abaqus FEA served as the ground truth metrics for the AI-predictive models generated in this study as described below.

2.2. U-NET convolution neural network (CNN)

The main objective of developing the U-NET was to train a model to automatically segment medical images, the initial step that is required before 3D surface reconstruction of the aneurysm wall and lumen. A U-NET (a type of convolutional neural network, CNN) that utilizes Keras (Version 2.4.0, Open-ended Neuro-Electronic Intelligent Robot Operating System, Google, Mountain View, CA) and Tensorflow (Google, Mountain View, CA) open source software libraries that are widely used in biomedical image-based applications (Ronneberger, Fischer, and Brox, 2015) was trained to automatically segment AAA ROI from medical image sets due to the U-NET's ability to segmented pixel borders. A clinical expert adjudicated and verified that the manual segmentations were representative ground truth images that defined the lumen, ILT, and aneurysm wall. There was a total of 10 unique AAA patient image sets with ground truth images corresponding to each axial slice of the entire dataset. Two dimensional axial slices (448 images) were used to construct a training set for the U-NET image classifier. Each axial image had a raster size of 512 by 512 pixels that were associated with their corresponding ground truth mask that was manually segmented. Training was performed using a custom python script for U-NETs and implemented on both a local workstation optimized for multi-GPU training with four NVIDIA (NVIDIA Inc., Santa Clara, CA) 2080TI's graphics cards and an Amazon Web Services Elastic Computing Node EC2 (Amazon Inc., Seattle, WA). The optimization of the U-NET classifier was performed altering training parameters that included the sub-image pixel size, the number of sub-images for the entire training set, and the number of epochs. The final trained U-NET included 3.5 million sub-images with an initial patch size of 36 by 36 pixels with 500 epochs. After the U-NET was trained, the test data was input and additional performance metrics were calculated by comparing the predicted image with ground truth images using accuracy, precision, sensitivity and specificity.

Each AAA image set was input into our trained U-NET model for automatic segmentation, and a post-processing script was used to extract the point cloud of the lumen and wall geometries. Point cloud geometries for the lumen and wall were converted into a preliminary mesh using triangular elements and Laplacian surface-preserving smoothing (Sousa et al., 2007) was applied. Several morphological indices were calculated for each mesh that includes AAA volume, ILT volume, average curvature, maximum diameter (normal to centerline), wall and lumen tortuosity to compare manually and automatically segmented geometries that were reconstructed. A two-sample t-test using unequal variances was used to compare morphological indices between the two groups (manual vs. automatic segmentation).

2.3. Finite element analysis of AAA

The FEA used in this study followed a well-established general process (Raghavan and Vorp, 2000, Vorp, 2007, Chung et al., 2017, Fillinger et al., 2003, Wang et al., 2002,

Doyle et al., 2013) and incorporates previously published, experimentally measured material properties of the aneurysm wall and ILT (Vande Geest et al., 2006, Vande Geest et al., 2006, Vande Geest et al., 2008, Wang et al., 2002). After the segmentation of the ROI, point clouds for the lumen and wall were converted into polysurfaces that were imported into ANSYS ICEM. There the geometries were meshed to incorporate both 2D shell elements for the wall/lumen geometries and 3D volumetric elements for the ILT. The final FEM model constructed utilized 2D shell elements (S3R) for the aneurysm wall, 3D tetrahedral elements (C3D8) for the ILT, hyperelastic isotropic ILT material properties, and a uniform AAA thickness wall of 1.9 millimeters (mm) with anisotropic material properties. Boundary conditions included the distal and proximal ends of the AAA being constrained in the X, Y, and Z directions and an ideal systolic pressure of 120 mmHg applied to the luminal surface. All simulations were performed in Abaqus Standard with Microsoft Visual Studio 2017 (Microsoft Inc., Redmond, WA) and Intel Fortran Compiler (Intel Inc., Santa Clara, CA) using a user-defined function to prescribe the anisotropic material properties of the wall.

2.4. Dataset preparation for training a machine learning regression model

ML was used to train a regression model to predict wall stresses. Datasets from the 10 AAA were prepared from the wall stress outputs of the FEA model along with morphological indices to train a ML regression model using Tree-Based Pipeline Optimization Tool (TPOT) targeting von Mises wall stress (Olson and Moore, 2019). The automatically segmented and manually segmented surface reconstructed geometries were prepared and input into the trained ML regression model to predict the wall stress distribution of AAA. Additional indices were calculated by using the wall surface nodes as a reference frame relative to the lumen surface nodes and centerline of each AAA and a dataset was constructed to train a predictive ML model. The wall and lumen surfaces were extracted from the Abaqus input file and the following indices were tabulated in columns for each wall node (rows): Cartesian coordinates (X,Y,Z) with the centroid of each geometry placed at the origin (0,0,0) through translation, minimized Euclidean distance from each wall node to lumen node representing intraluminal thrombus thickness, minimized Euclidean distance from the wall to the centerline representing the maximum circumferential radii, max and min principal curvatures for each wall node, and six closest nodal neighbors' principal curvatures in rank order from nearest to furthest distance providing a localized regional curvature map for each node Regions of the wall surface were labeled to identify the proximal and distal displacement boundary and each node's Euclidean distance to the nearest nodal boundary (Fig. 2). For example, the boundary nodes were labeled with '0' with striated regions in the proximal or distal direction labeled 1 through 5, with 5 being at the centroid of each aneurysm relative to the superior or inferior boundary. The nodal wall stresses from the Abaqus output file were input into the last column of the prepared dataset as the desired predictive output for regression modeling.

2.5. Machine learning regression modeling

The datasets that were prepared from a list of various morphological indices and the calculated wall stresses were used to train a ML regression model with the objective to be used for wall stress prediction. The prepared dataset of ten AAA cases with 253,823 nodes and 27 features (as prescribed in the dataset preparation) was input into an in-house

custom python script utilizing Tree-based Pipeline Optimization Tool (TPOT). TPOT is a type of Auto Machine Learning (AutoML) that tunes hyperparameters using python libraries (sci-kit learn and XGBoost) to export an optimized regression model that reflects the lowest cross-validation score. The model with the lowest cross-validation score was an Extra Tree Regressor and the trained model was exported. Prepared datasets from the manual and automated geometric reconstructions were input to the trained classifier to predict the wall stress distribution in each AAA, which were visualized in Paraview. A paired student t-test was performed using two biomechanical indices, the peak wall stress (99th percentile) and mean wall stress to quantitatively compare the FEA stress results (ground truth) with the ML-predicted wall stress data from both the manual and automated geometric reconstructions pipelines.

3. Results

The optimal U-NET classifier was trained with 448 images, 3.5 million sub-images and 500 epochs and the training axial slices were input resulting in 99.8% accuracy, 97.2% precision, 96.0% sensitivity and 99.9% specificity. Fig. 3 displays the precision-recall curve, receiver operator characteristics (ROC) curve of the trained automated segmentation classifier, and the qualitative results of the predicted automatic segmentation of the ILT region. There was no statistical difference ($p > 0.05$) between the manually and automatically segmented geometries using the calculated morphological indices between the manually and automatically segmented geometries.

The prepared datasets from automatic and manual segmentation of all AAA were input into the trained ML model (Extra Tree Regressor) to produce the predicted wall stress values that are displayed in Fig. 4. Comparisons were made between the FEA wall stress results and the predicted wall stresses using both the manually and automatically segmented geometries (Fig. 5). The ground truth FEA-calculated stresses revealed a peak wall stress of 24.7 ± 3.80 N/cm^2 and a mean wall stress of 9.51 ± 1.81 N/cm^2 (averaged across all ten AAA). For the ML-predicted wall stresses using the original manually segmented AAA geometries and their respective morphological features we found a peak of 25.4 ± 3.60 N/cm^2 and a mean of 10.1 ± 1.92 N/cm^2, which exhibited an R^2 of 0.99 and 0.997 when compared to the ground truth. For the ML-predicted wall stresses using the AI-assisted segmented AAA geometries and their respective morphological features we found a peak of 26.3 ± 2.64 N/cm^2 and a mean of 8.42 ± 1.16 N/cm^2, or an R^2 of 0.840 and 0.860 when compared to the ground truth.

It was also measured that on average that it took ~20 seconds to perform the automated image segmentation, conversion of the point clouds to the prepared dataset, and prediction of wall stresses for each aneurysm. Whereas it takes about 4 hours on average per patient specific AAA to perform the traditional pipeline that requires manual segmentation, meshing, finite element analysis, and post-processing.

4. Discussion

In this study, a new AI framework was compared to a traditional workflow in terms of reconstructing AAA geometries and calculating wall stresses within patient AAAs. It was

found that the trained U-NET performing automatic segmentation produced a 3D surface reconstructed geometry statistically no different to the manually constructed geometry (Table 1) and with regards to a list of morphological indices that included maximum diameter (normal to centerline), asymmetry factor, aneurysm tortuosity, aneurysm surface area, AAA volume, ILT Volume, and mean curvature. However, the ILT volume had the highest percent mean difference between manual and automated segmentation approach due to the inability of the U-NET to appropriately predict the boundary fo the aneurysm wall. Morphological features were tabulated and prepared for training a ML regression model for predicting AAA wall stresses, using those derived from FEA as the ground truth or predicted output. There was no qualitative or statistical difference when either the automatically segmented or manually segmented ground truth geometries were input into the wall stress prediction regression model (Figs. 4 and 5, respectively).

Previous studies have investigated the relationships between wall stress and either localized morphological features (curvatures (Sacks et al., 1999, Martufi et al., 2009), ILT thicknesses (Vande Geest et al., 2006, Wang et al., 2002), wall thicknesses (Chung et al., 2017, Doyle et al., 2008)) or global morphological features (maximum diameter (Vorp, Raghavan, and Webster, 1998), volume (Wang et al., 2002, Martufi et al., 2013), asymmetry (Doyle et al., 2009, Vorp, Raghavan, and Webster, 1998), ILT volume (Wang et al., 2002)). Soudah et al., 2015 proposed a method to predict the mechanical stress in AAA using neural networks but relied on idealized geometries without the presence of ILT and anisotropic material models. There has not been, to our knowledge, any attempts to perform AAA wall stress predictions using a ML model trained with FEA stress results from a finite element model that incorporates anisotropic wall and ILT material properties (Vande Geest et al., 2008). In studies investigating principal curvatures, a correlation between principal wall stresses can be seen when ILT is omitted (Sacks et al., 1999). Therefore, it stands to reason that the use of ML regression models in conjunction with additional morphological features is more robust in the prediction of wall stresses than solely relying on localized surface features of the aneurysm wall.

The initial results of this study are promising, but there are several limitations and challenges to overcome for future studies. The automatically segmented ILT volume was overestimated when compared to manually segmented surface reconstructions. This is directly related to the performance of the U-NET, and an unintended consequence of using medical images of varying quality (slice thickness relating to number of images per 3D stack). Future work will improve the U-NET by using a large GPU accelerated supercomputing platform to accommodate more data in the model used for automatic segmentation. Training the ML regression models relied on a model with the highest internal cross validation score using 10% of the entire dataset. The relatively small sample size (n = 10) and the trained model was only tested on the AAA surface reconstructions from the automated pipeline. Additional studies will include inputting a new dataset of patient medical images (that were not used during training) into the stress prediction pipeline to increase the sample size and data variability to assess and improve the overall AI framework tools. Future studies will expand on the number of training cases to further validate the U-NET and ML model that will provide accurate stress predictions of AAA geometries.

Traditional methods to perform geometric reconstruction and finite element analysis of AAA require a substantial commitment of time (hours per AAA), money, and expert personnel. For the AI framework presented here, average process times per AAA were only 15 seconds for the automatic segmentation (using a single NVIDIA 2080Ti GPU) and 5 seconds for the wall stress predictions. Furthermore, we propose that this framework will have utility to other soft tissue organs and structures where mechanical stress is linked to disease propagation and poor patient outcomes (e.g., thoracic aortic and cerebral aneurysms, heart valves, ligaments, etc.).

5. Conclusion

Our AI framework was shown here to enable 3D reconstruction of the complexly shaped AAA and prediction of biomechanical wall stresses acting on them much more rapidly than traditional manual reconstruction and FEA. Our results suggest that AI can be employed to reliably perform these tasks, which would lend itself to large-scale high-throughput biomechanical studies of AAA that are lacking in the literature. The approach could easily be adapted to allow for similar analyses of other organs and disease states.

Acknowledgments

Abbreviations:

AAA	Abdominal Aortic Aneurysm
AI	Artificial Intelligence
CNN	Convolutional Neural Network
DICOM	Digital Imaging and Communication
FEA	Finite Element Analysis
ILT	Intraluminal Thrombus
ML	Machine Learning

References

Chung TK, da Silva ES, Raghavan SML, 2017. Does elevated wall tension cause aortic aneurysm rupture? Investigation using a subject-specific heterogeneous model. J. Biomech 64, 164–171. [PubMed: 29102265]

Di Martino ES, Vorp DA, 2003. Effect of variation in intraluminal thrombus constitutive properties on abdominal aortic aneurysm wall stress. Ann. Biomed. Eng 31, 804–809. [PubMed: 12971613]

Doyle BJ, et al. , 2008. 3D reconstruction and manufacture of real abdominal aortic aneurysms: From CT scan to silicone model. J. Biomech. Eng 130.

Doyle BJ, et al. , 2009. Vessel asymmetry as an additional diagnostic tool in the assessment of abdominal aortic aneurysms. J. Vasc. Surg 49, 443–454. [PubMed: 19028061]

Doyle BJ, Callanan A, Grace PA, Kavanagh E, 2013. On the influence of patient-specific material properties in computational simulations: A case study of a large ruptured abdominal aortic aneurysm on the influence of patient-specific material properties in computational simulations: A case study of a large. Int. J. Numer. Method Biomed. Eng 26, 807–827.

Fillinger MF, Marra SP, Raghavan ML, Kennedy FE, 2003. Prediction of rupture risk in abdominal aortic aneurysm during observation: Wall stress versus diameter. J. Vasc. Surg 37, 724–732. [PubMed: 12663969]

Fillinger MF, Raghavan ML, Marra SP, Cronenwett JL, Kennedy FE, 2002. In vivo analysis of mechanical wall stress and abdominal aortic aneurysm rupture risk. J. Vasc. Surg 36, 589–597. [PubMed: 12218986]

Georgakarakos E, et al. , 2010. The Role of Geometric Parameters in the Prediction of Abdominal Aortic Aneurysm Wall Stress. Eur. J. Vasc. Endovasc. Surg 39, 42–48. [PubMed: 19906549]

Holzapfel GA, 2006. Determination of material models for arterial walls from uniaxial extension tests and histological structure. J. Theor. Biol 238, 290–302. [PubMed: 16043190]

Khosla S, Morris DR, Moxon JV, 2015. Meta-Analysis of Peak Wall Stress in Ruptured, Symptomatic, and Intact Abdominal Aortic Aneurysms. J. Vasc. Surg 61, 836–837.

Chen Tianqi, and Guestrin Carlos. "XGBoost: A Scalable Tree Boosting System." Proceedings of the 22nd ACM SIGKDD International Conference on Knowledge Discovery and Data Mining. ACM, 2016. 785–794. Web.

López-Linares K, García I, García-Familiar A, Macía I & Ballester MAG 3D convolutional neural network for abdominal aortic aneurysm segmentation. (2019).

Kontopodis Nikolaos, Pantidis Dimitrios, Dedes Athansios, Daskalakis Nikolaos, Ioannou Christos, 2016. The – Not So – Solid 5.5 cm Threshold for Abdominal Aortic Aneurysm Repair: Facts, Misinterpretations, and Future Directions. frontiers in surgery 3 (January). 10.3389/fsurg.2016.00001. In press.

Maier A, et al. , 2010. A comparison of diameter, wall stress, and rupture potential index for abdominal aortic aneurysm rupture risk prediction. Ann. Biomed. Eng 38, 3124–3134. [PubMed: 20480238]

Martufi G, et al. , 2013. Multidimensional growth measurements of abdominal aortic aneurysms. J. Vasc. Surg 58, 748–755. [PubMed: 23611712]

Martufi G, Di Martino ES, Amon CH, Muluk SC, Finol EA, 2009. Three-dimensional geometrical characterization of abdominal aortic aneurysms: image-based wall thickness distribution. J. Biomech. Eng 131, 061015. [PubMed: 19449969]

Olson RS & Moore JH TPOT: a tree-based pipeline optimization tool for automating machine learning. in (2019). doi:10.1007/978-3-030-05318-5_8.

Raghavan ML, Fillinger MF, Marra SP, Naegelein BP, Kennedy FE, 2005. Automated methodology for determination of stress distribution in human abdominal aortic aneurysm. J. Biomech. Eng 127, 868. [PubMed: 16248318]

Raghavan ML, Vorp DA, 2000. Toward a biomechanical tool to evaluate rupture potential of abdominal aortic aneurysm: Identification of a finite strain constitutive model and evaluation of its applicability. J. Biomech 33, 475–482. [PubMed: 10768396]

Raghavan ML, Vorp DA, Federle MP, Makaroun MS, Webster MW, 2000. Wall stress distribution on three-dimensionally reconstructed models of human abdominal aortic aneurysm. J. Vasc. Surg 31, 760–769. [PubMed: 10753284]

Raghavan ML, Webster MW, Vorp DA, 1996. Ex vivo biomechanical behavior of abdominal aortic aneurysm: assessment using a new mathematical model. Ann Biomed Eng 24, 573–582. [PubMed: 8886238]

Reeps C, et al. , 2013. Measuring and modeling patient-specific distributions of material properties in abdominal aortic aneurysm wall. Biomech. Model. Mechanobiol 12, 717–733. [PubMed: 22955570]

Ronneberger O, Fischer P, Brox T, 2015. U-net: Convolutional networks for biomedical image segmentation. In: Lecture Notes in Computer Science (including subseries Lecture Notes in Artificial Intelligence and Lecture Notes in Bioinformatics). 10.1007/978-3-319-24574-4_28.

Sacks MS, Sun W, 2003. Multiaxial mechanical behavior of biological materials. Annu. Rev. Biomed. Eng 5, 251–284. [PubMed: 12730082]

Sacks MS, Vorp DA, Raghavan ML, Federle MP, Webster MW, 1999. In vivo three-dimensional surface geometry of abdominal aortic aneurysms. Ann. Biomed. Eng 27, 469–479. [PubMed: 10468231]

Shum J, et al. , 2011. Quantitative assessment of abdominal aortic aneurysm geometry. Ann. Biomed. Eng 39, 277–286. [PubMed: 20890661]

Soudah Eduardo, Rodríguez Jo e, López Roberto, 2015. Mechanical Stress in Abdominal Aortic Aneurysms Using Artificial Neural Networks. Journal of Mechanics in Medicine and Biology 15 (3).

Sousa FS, Castelo A, Nonato LG, Mangiavacchi N, Cuminato JA, 2007. Local volume-conserving free surface smoothing. Commun. Numer. Methods Eng 23, 109–120.

Tierney ÁP, Callanan A, McGloughlin TM, 2012. Use of regional mechanical properties of abdominal aortic aneurysms to advance finite element modeling of rupture risk. J. Endovasc. Ther 19, 100–114. [PubMed: 22313210]

Truijers M, et al. , 2007. Wall stress analysis in small asymptomatic, symptomatic and ruptured abdominal aortic aneurysms. Eur. J. Vasc. Endovasc. Surg 33, 401–407. [PubMed: 17137809]

Vande Geest JP Towards an improved rupture potential index for abdominal aaneurysms: anisotropic constitutive modeling and noninvasive wall strength estimation. 317 (2005).

Vande Geest JP, Di Martino ES, Bohra A, Makaroun MS, Vorp DA, 2006. A biomechanics-based rupture potential index for abdominal aortic aneurysm risk assessment: demonstrative application. Ann. N. Y. Acad. Sci 1085, 11–21. [PubMed: 17182918]

Vande Geest JP, Sacks MS, Vorp DA, 2006. The effects of aneurysm on the biaxial mechanical behavior of human abdominal aorta. J. Biomech 39, 1324–1334. [PubMed: 15885699]

Vande Geest JP, Schmidt DE, Sacks MS, Vorp DA, 2008. The effects of anisotropy on the stress analyses of patient-specific abdominal aortic aneurysms. Ann. Biomed. Eng 36, 921–932. [PubMed: 18398680]

Vorp DA, 2007. Biomechanics of abdominal aortic aneurysm. J. Biomech 40, 1887–1902. [PubMed: 17254589]

Vorp DA, 2009. Biomechanics of abdominal aortic aneurysms. J. Biomech 40, 1887–1902.

Vorp DA, Raghavan ML, Webster MW, 1998. Mechanical wall stress in abdominal aortic aneurysm: Influence of diameter and asymmetry. J. Vasc. Surg 27, 632–639. [PubMed: 9576075]

Wang DHJ, Makaroun MS, Webster MW, Vorp DA, 2002. Effect of intraluminal thrombus on wall stress in patient-specific models of abdominal aortic aneurysm. J. Vasc. Surg 36, 598–604. [PubMed: 12218961]

Wang D et al. Neural network fusion: a novel CT-MR aortic aneurysm image segmentation method. 75 (2018) doi:10.1117/12.2293371.

Zhang H, Kheyfets VO, Finol EA, 2013. Robust infrarenal aortic aneurysm lumen centerline detection for rupture status classification. Med. Eng. Phys 35, 1358–1367. [PubMed: 23608300]
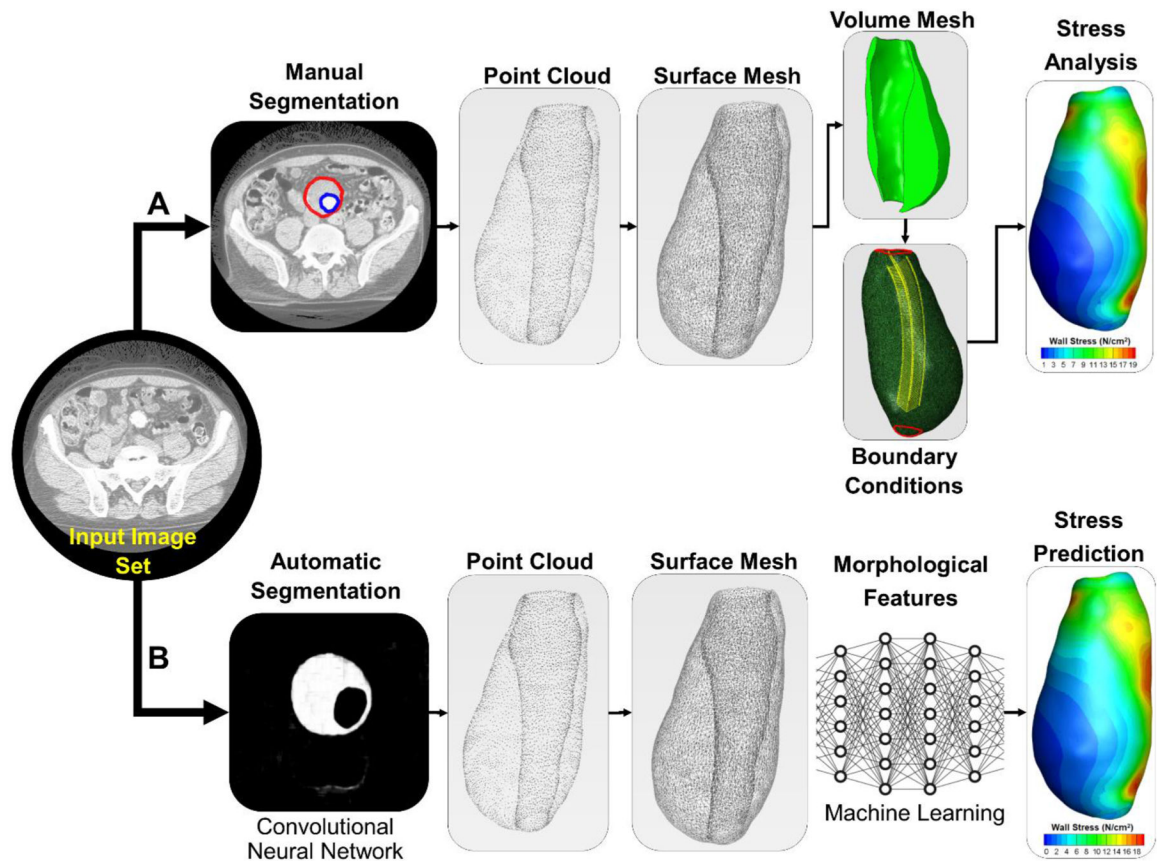
Fig. 1.
Overview of the two methods used to assess the biomechanical status of an abdominal aortic aneurysm. **A)** Traditional pipeline for stress analysis of AAA includes image segmentation to finite element analysis. This pipeline requires manual segmentation from an input AAA image stack, point cloud generation, surface meshing, volumetric meshing, and generation of a FEA model with appropriate boundary conditions, material properties and loading conditions. **B)** AI framework to predict the wall stresses on a given AAA. This approach utilizes a convolution neural network for automatic segmentation, point cloud generation, surface mesh generation, input of morphological features, and then training a Machine Learning (ML) Regression model.
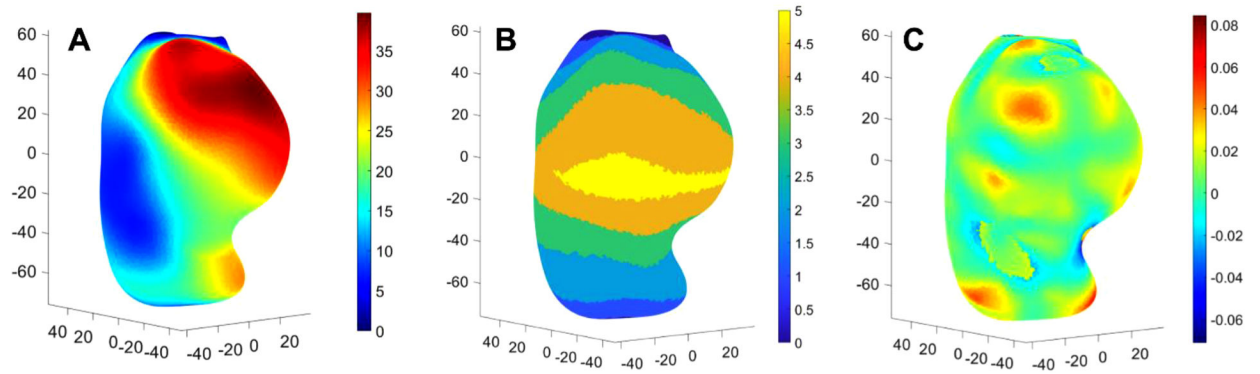
Fig. 2.
Several key morphological features that are extracted for each reconstructed aneurysm surface. **A)** Intraluminal thrombus (ILT) thickness in millimeters (mm) represented on the surface of a sample reconstructed AAA. **B)** Regional striping of the aneurysm in five distance zones ranging from 0 to 5, representing the distance away from the proximal and distal boundaries of the aneurysm. Region 5 is the maximum distance away from either boundary while Region 0 represents the proximal or distal boundaries. **C)** Map of the localized maximum principal curvature on the surface of the AAA (1/mm).
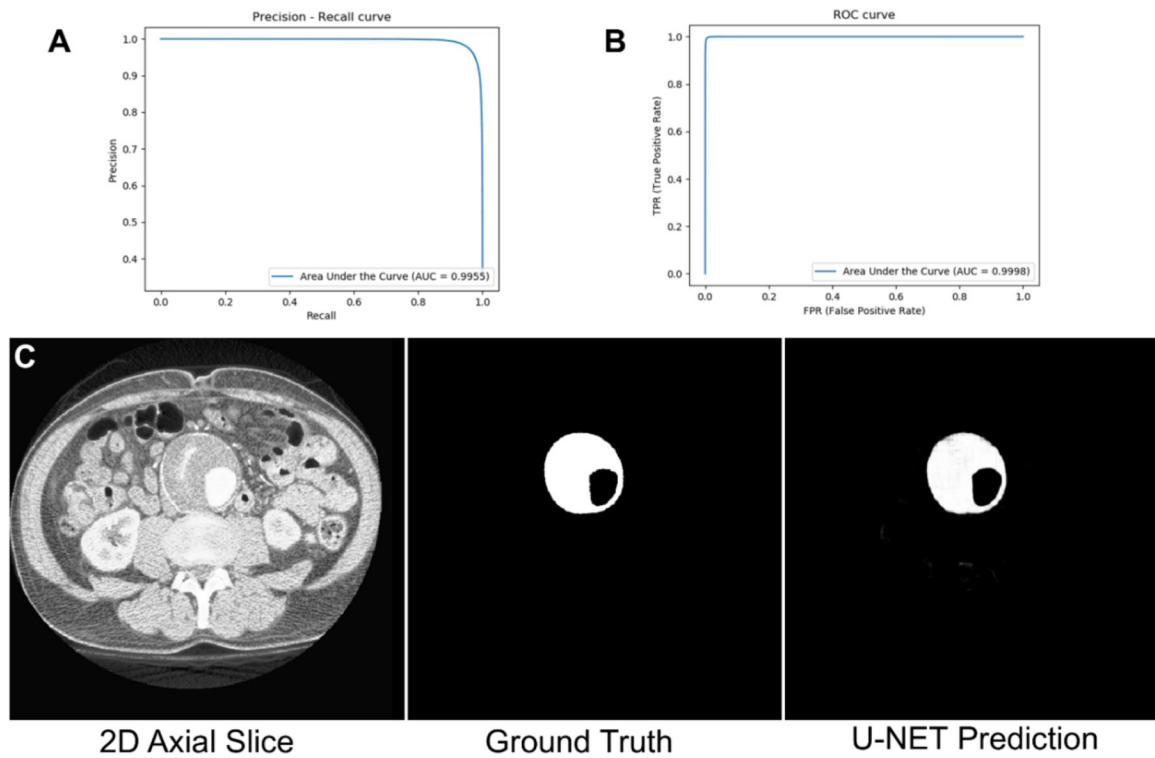
Fig. 3.
Assessment of the performance of the trained U-NET image classifier. **A)** Precision –
Recall curve of the trained U-NET (Area under the curve 0.996). **B)** Receiver Operator
characteristic curve of the trained U-NET (area under the curve 0.999). **C)** Qualitative
results of a single axial AAA slice with ground truth and U-NET prediction.
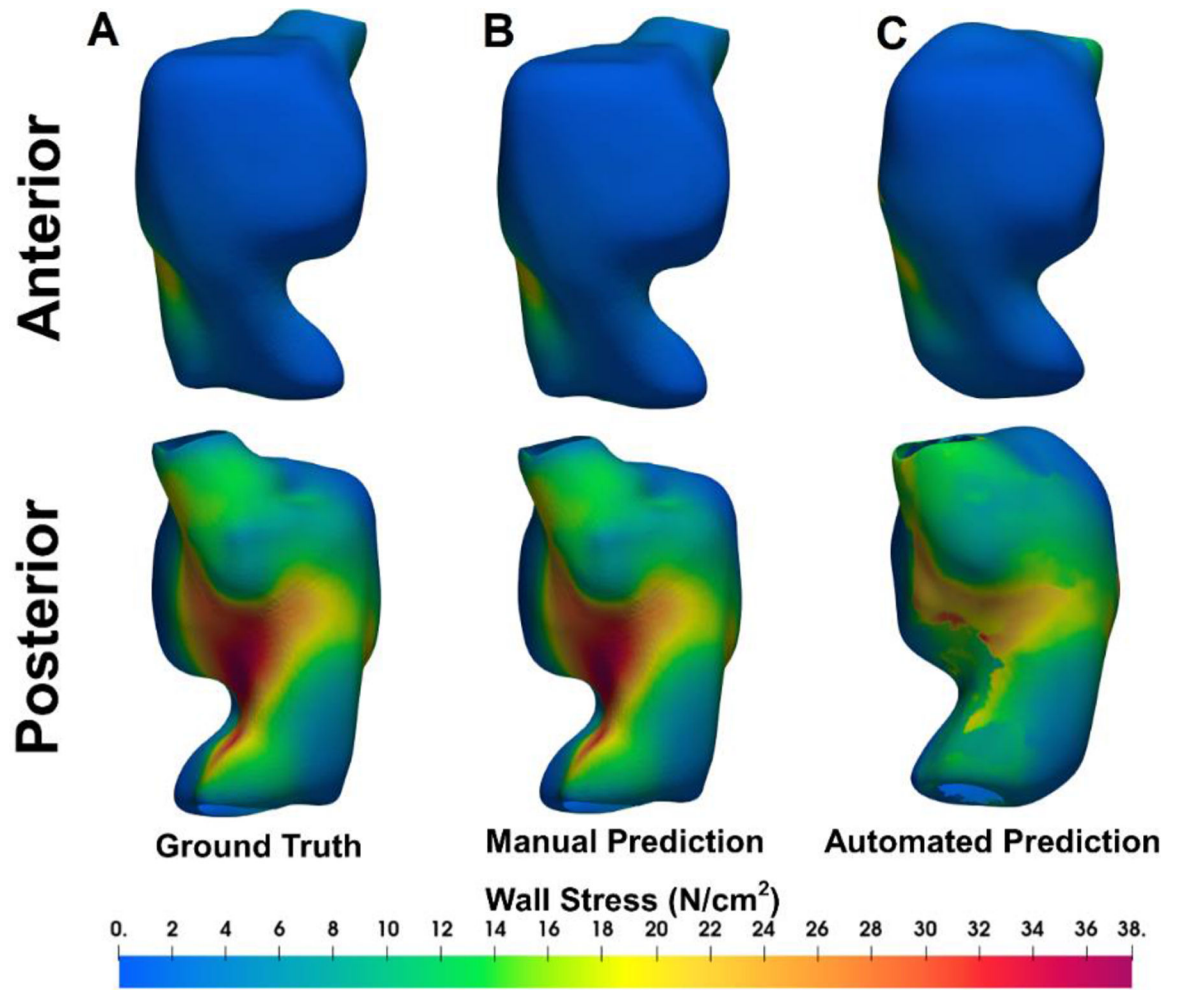
Fig. 4.
Wall stress maps for a representative AAA obtained using FEA (ground truth, **A**), and predicted using the trained ML model with the manually segmented geometry (**B**) and with the automatically segmented geometry (**C**).
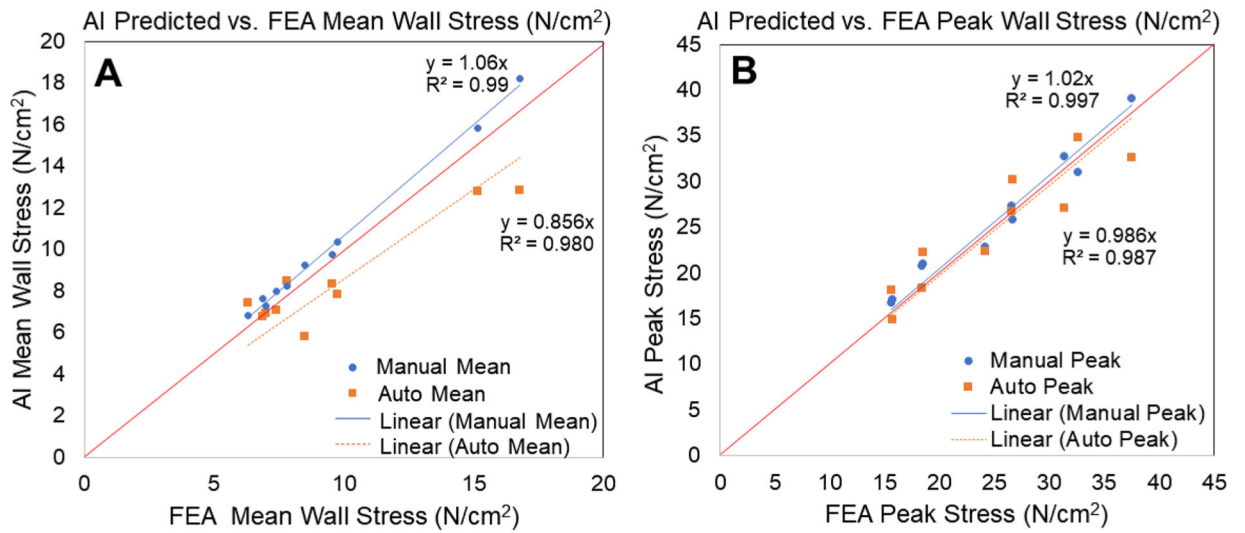
Fig. 5.
Comparison of AI- and FEA-predicted mean (**A**) and peak/99th percentile (**B**) wall stresses for all 10 AAA cases. For AI-predicted stresses, results are shown for using both manually- and automatic-segmented geometries.

Table 1

Comparison of Morphological Indices in Manual and Automated AAA 3D surface Reconstructions

Morphological index	Manual AAA geometries	Automated AAA geometries	% Difference of mean	p-value
Maximum Diameter (cm)	6.6 ± 2.2	6.2 ± 1.44	7.02%	0.60
Asymmetry Factor	0.85 ± 0.082	0.80 ± 0.110	5.10%	0.33
Aneurysm Tortuosity	1.24 ± 0.108	1.17 ± 0.110	5.76%	0.16
Aneurysm Surface Area (cm^2)	194.5 ± 88.6	179.1 ± 62.4	7.29%	0.88
AAA Volume (cm^3)	193.0 ± 171.8	183.2 ± 108.0	5.06%	0.66
ILT Volume (cm^3)	91.9 ± 92.2	119.1 ± 85.0	29.6%	0.50
Mean Curvature (mm^{-1})	0.031 ± 0.0064	0.035 ± 0.0084	7.92%	0.26